



# Parameter optimization of a micro-textured ball-end milling cutter with blunt round edge

Shucai Yang<sup>1</sup> · Wei Ren<sup>1</sup> · Tianjiao Wang<sup>1</sup> · Shuai Su<sup>1</sup>

Received: 8 June 2019 / Accepted: 20 September 2019 / Published online: 23 November 2019  
© Springer-Verlag London Ltd., part of Springer Nature 2019

## Abstract

Titanium alloys is a typical difficult-to-cut material with many machining problems, build-up-edge, large cutting force, and high cutting heat. Previous research has shown that micro-texture on the tool surface can solve the above problems potentially, and that a blunt round edge of the cutting tool can enhance its strength and improve the tool wear resistance. Therefore, towards an optimal parameter of micro-texture and blunt round radius, a finite element method (FEM) simulation and an experiment are carried out, where the test result provides a set of data for a genetic algorithm-based prediction model. The optimized parameter combinations of the micro-textured ball-end milling cutter with a blunt round edge are obtained and compared in a set of experiments. The optimized parameters refer to a 40- $\mu\text{m}$  radius of the blunt round edge, a 40- $\mu\text{m}$  micro-texture diameter, a 175- $\mu\text{m}$  spacing, a 120- $\mu\text{m}$  distance from the cutting edge, and an 80- $\mu\text{m}$  depth.

**Keywords** Ball-end mill · Blunt round edge · Micro-texture · Genetic algorithm

## 1 Introduction

Because titanium alloys is equipped with many advantages, such as high specific strength and corrosion resistance, it has been applied to many fields, e.g., aviation and aerospace. From raw material to components of titanium alloys, milling is one of the most important processes, where the freeform surface is machined by using a ball-end mill, e.g., impeller blades. However, titanium alloys generally are considered a difficult-to-cut material; therefore, there are some machining difficulties, e.g., large cutting force, high cutting temperature, high stickiness on tools, and short tool life. To solve the problems, much research has been done, in which a blunt round edge could improve cutting edge strength of the tool and slow down tool wear, and a micro-textured rake face of a cutting tool could reduce cutting forces and improve the machining surface [1–3].

A blunt round edge of the cutting tool affects the formation and flow direction of chips and has a significant impact on the cutting performance [4, 5]. Obikawa et al. [6] carried out a set

of finite element method (FEM) simulations and experiments of face milling of a titanium alloy; of which, results showed that a blunt edge plays an important role in increasing the tool edge strength and in reducing tool wear. Wan et al. [7] simulated a cutting process by a micro-structure of the cutting edge of a coated tool on ABAQUS. Their results showed that the radial force and cutting temperature are increased with increasing the radius of a blunt round edge. Cao et al. [8] studied the influence of the blunt radius of the tool on the size effect of tool by using ABAQUS FEM. The results showed that the existence of blunt circular edge makes the cutting rake angle a negative rake angle, which leads to the enhancement of plowing effect, increases the energy loss, and affects the processing quality of the machined surface of the workpiece. Ezugwu et al. [9] optimized the blunt round edge of a PVD-coated tool and proved that a blunt round edge can improve the tool life. Kawasegi et al. [10] developed a new cutting tool based on the theory of slip line field. It was observed that the blunt round edge of the tool enhanced the size effect, and the shear fluidity was changed under different blunt round edges. Wu [11] focused on the mechanism of the blunt round cutting edge. Through theoretical calculation and experimental analyses, it was observed that the depth and degree of cold hardening of the surface layer increase with the increase of the radius of the blunt round edge, resulting in large compressive residual stress in the surface layer, which can improve the

✉ Shucai Yang  
yangshucai@hrbust.edu.cn

<sup>1</sup> School of Mechanical and Power Engineering, Harbin University of Science and Technology, Harbin 150080, China

wear resistance and fatigue strength of the surface but make the low rigidity parts easy to be deformed. She et al. [12] analyzed the influence of the radius of blunt round edge on milling temperature by using AdvanEdge. Their results showed that the milling temperature increases as the radius of the cutting edge increases.

The micro-texture on the tool refers to a lattice pattern including pits or minute grooves on tool functional surfaces. General geometric shapes include circular, rectangular, and hexagonal pits, and parallel or mesh-shaped grooves [13]. Enomoto and Sugihara [14–16] used femtosecond laser processing technology to process micro-texture on the rake face of coated tools and tested the tools in a set of experiments. The study showed that the cutting force and cutting temperature can be reduced since the micro-texture stored lubricating fluid which reduced tool-to-chip contact area. Enomoto and Sugihara [17, 18] processed the micro-groove texture on the working surface of a cutting tool and observed that the crater wear on the rake face of the cutting tool can be improved significantly. Applying the micro-texture anti-friction and anti-wear properties to the flank face also reduces the wear of the flank face. Koshy et al. [19] experimentally proved that machining continuous and array micro-textures on the rake face of high-speed steel tools can store cutting fluid and reduce the main cutting force and feed force. Wu et al. [20] machined micro-nano structure friction reduction groove on the tool rake face by laser technology. After the cutting test, it was shown that the friction-reducing groove can reduce cutting force and improve the cutting performance of the tool. Yin et al. [21] conducted a chamfering experiment on a stainless steel as a 3C product shell based on the grinding side “V”-shape texture. The results show that a suitable combination of texture types and texture angles can provide a significant improvement of tool life and surface quality. Yang et al. [22] established the simulation model of the micro-texture surface of cemented carbide by using ABAQUS FEM. The results show that the micro-texture can absorb stress and change the status of stress distribution on the surface, and the performance of micro-pit is the best one. Li et al. [23] studied the cutting performance of two different types of cutting tools by using multi-level fuzzy comprehensive evaluation method based on multi-objective decision theory. The results show that the micro-structure of the surface has wear resistance and can store impurities.

The cutting edge passivation and the micro-texture on tool surfaces can improve the cutting performance of the tool. However, it is not clear how the multi factors of cutting edge and micro-texture influence cutting performance. Therefore, towards such goals, this paper investigates the cutting performance of the ball-end mill with both the blunt round edge and surface micro-texture by using FEM and experiments. Then, a prediction model for milling force is established based on genetic algorithm (GA). Finally, the optimal parameter

combination of the micro-textured ball-end milling cutter with a blunt round edge is obtained, which is validated by a separate experiment.

## 2 FEM simulation

A software, DEFORM-3D, is used to perform FEM simulation. The radius of blunt round edge, and diameter of pit, spacing between pits, distance to cutting edge, and depth of pit are under consideration. To cover those parameters, a Taguchi method is employed, and 25 inserts are designed, as shown in Table 1. The 3D models of those inserts are established in Siemens NX 10.0, as shown in Fig. 1. The other parameters of the tool are as follows: the rake angle is  $0^\circ$ , the back angle is  $11^\circ$ , and the tool diameter is 20 mm. The size of the workpiece model is  $15\text{ mm} \times 10\text{ mm} \times 5\text{ mm}$  with a  $15^\circ$  inclination angle. The relative location relationship of the insert and workpiece is shown in Fig. 2.

The 25 ball-end mill insert models with different blunt round edge radii and micro-texture parameters and workpiece models are imported into DEFORM-3D, and then tools and the workpiece are meshed, as shown in Fig. 3, where to obtain the accuracy, the mesh in the cutting zone is reshaped with a much smaller shape, and their state before and after the mesh reshaping is shown in Figs. 3a and b, respectively. A YG8 series cemented carbide composed of 92% WC and 8% Co is selected as tool material, and a Ti6Al4V is selected as the workpiece material. The cutting parameters are  $v_c = 120\text{ m/min}$ ,  $f_z = 0.08\text{ mm}$ ,  $a_e = 0.3\text{ mm}$ , and  $a_p = 0.5\text{ mm}$ . Figure 4 shows the simulated results, and cut-in state, intermediate state, and cut-out state of the tool are shown in Figs. 4a, b, and c, respectively.

Joint cutting force is used to evaluate the tool parameters. The results of the cutting force of 25 inserts are shown in Fig. 5. The range analysis of the milling force is also carried out, of which results are shown in Table 2. In terms of their influence on the milling force, blunt round edge radius is the biggest one, followed by diameter, distance to cutting edge, spacing, and depth, as shown in Fig. 6. Therefore, the cutting edge radius of a tool is the most sensitive factor to be considered in terms of the cutting force. The best combination of parameters is  $K_2R$ ,  $K_2D$ ,  $K_5L_2$ ,  $K_4L_1$ ,  $K_5H$ , i.e., a 40- $\mu\text{m}$  blunt round edge radius, a 40- $\mu\text{m}$  micro-texture diameter, a 200- $\mu\text{m}$  spacing, a 130- $\mu\text{m}$  distance to cutting edge, and an 80- $\mu\text{m}$  depth.

## 3 Experiment

### 3.1 Experimental setup

The selected inserts and workpiece in this experiment are the same as those in the simulation in Section 2, and their

**Table 1** Orthogonal test table

	Blunt round edge parameter		Micro-texture parameters/ $\mu\text{m}$			
	Radius/ $\mu\text{m}$		Diameter	Spacing	Distance from the cutting edge	Depth
1	20		30	125	90	40
2	20		40	150	100	50
3	20		50	175	110	60
4	20		60	200	120	70
5	20		70	225	130	80
6	40		30	150	110	70
7	40		40	175	120	80
8	40		50	200	130	40
9	40		60	225	90	50
10	40		70	125	100	60
11	60		30	175	130	50
12	60		40	200	90	60
13	60		50	225	100	70
14	60		60	125	110	80
15	60		70	150	120	40
16	80		30	200	100	80
17	80		40	225	110	40
18	80		50	125	120	50
19	80		60	150	130	60
20	80		70	175	90	70
21	100		30	225	120	60
22	100		40	125	130	70
23	100		50	150	90	80
24	100		60	175	100	40
25	100		70	200	110	50

parameters are shown in Table 1. The insert model is BNM-200, the tool holder model is BNML-200105S-S20C, and its total length is 141 mm. The micro-textures on the ball-end mill insert are machined in a laser mark machine, and two examples are shown in Fig. 7.

During the laser preparation of those micro-textures, the high temperature generated by the laser causes a serious ablation phenomenon on the surface of the tool, and a slag is formed around the pits of the micro-texture, as shown in Fig. 8, which may affect the tool's performance. Therefore, in order to minimize the influence, an additional process is needed; in this case, polishing is performed on the laser-processed surface. The morphology after treatment of micro-textured surface is shown in Fig. 9; the surface around the pit is improved.

In terms of blunt round edges of those inserts, a sandblasting method is used, of which processes are shown in Fig. 10. The abrasive used in this experiment is quartz sand. A different radius of the cutting edge is shown in Fig. 11a–c, respectively.

A rough face milling is used, and its setup is shown in Fig. 12. The employed cutting parameters are the same with those

in FEM in Section 2, measuring the milling force with rotating force gauge.

### 3.2 Analysis on the milling force

Figure 13 shows the cutting force result of all the 25 inserts. It is evident that the milling force is the smallest under the experiment of number 7. The parameters refer to a 40- $\mu\text{m}$  radius of the blunt round edge, a 40- $\mu\text{m}$  micro-texture diameter, a 175- $\mu\text{m}$  spacing, a 120- $\mu\text{m}$  distance from the cutting edge, and an 80- $\mu\text{m}$  depth.

The variation trend of the simulated milling force is similar with the variation of the experimentally measured milling force, as shown in Fig. 14. The measured milling forces in the experiment are significantly larger than the milling force obtained in the simulation, which is caused due to the following: (1) the workpiece and the tool cannot be fully and thoroughly meshed and (2) the friction between the tool flank and the workpiece is neglected.

The range analysis method is used to analyze the milling force data, of which results are shown in Table 3. The blunt round edge radius has the biggest influence on the cutting

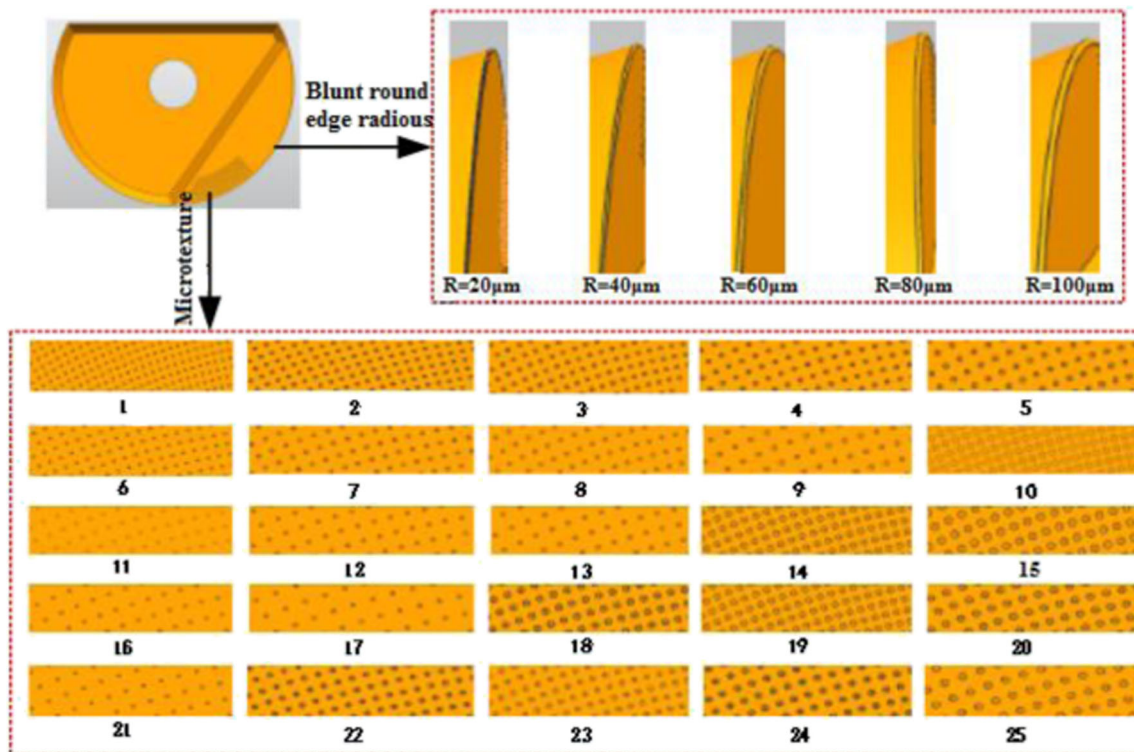
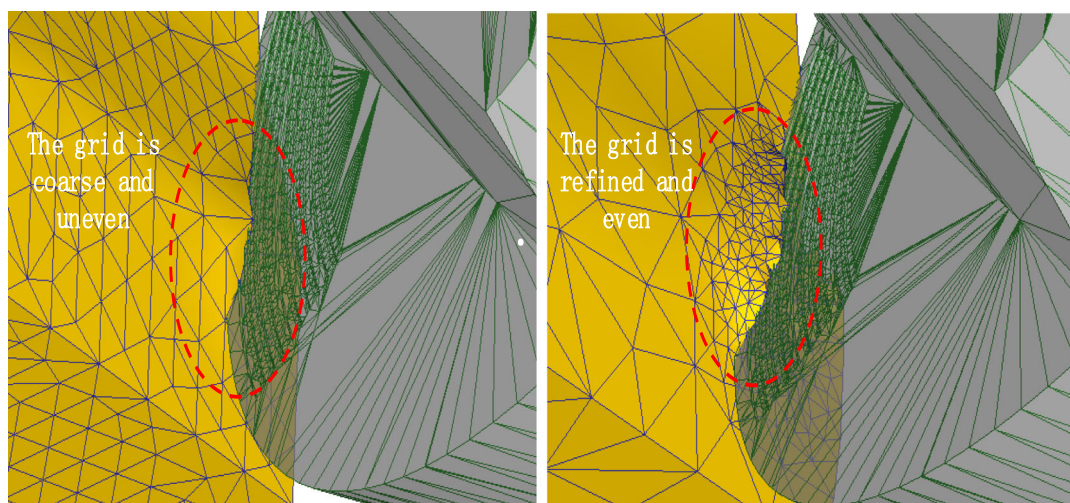
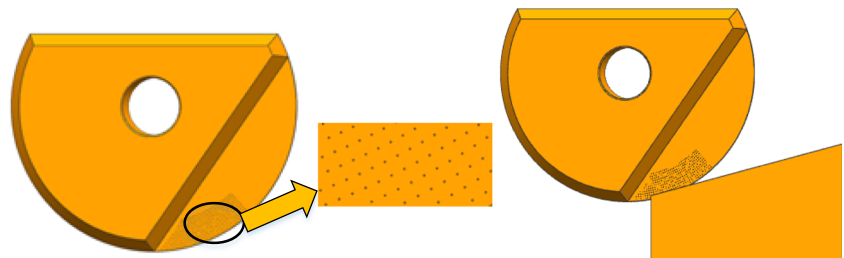


Fig. 1 The 3D models of the 25 inserts and their blunt edge radius and micro-textures

Fig. 2 Micro-textured cutting tool and its assembly relationship with the workpiece



a) Before the local refinement of the mesh b) After the local refinement of the mesh

Fig. 3 Comparisons before and after mesh reshaping. a Before the local refinement of the mesh; b after the local refinement of the mesh

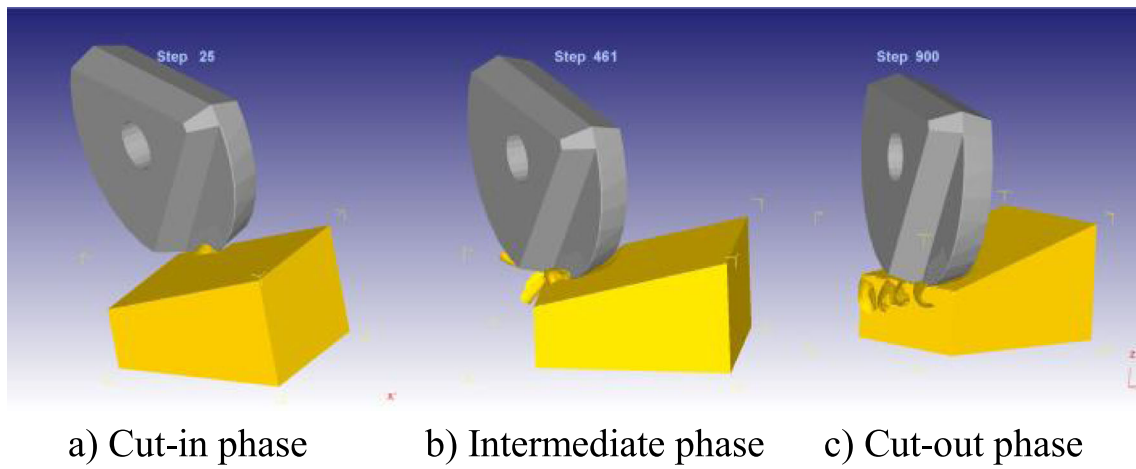


Fig. 4 Cutting simulation of micro-textured cutting tool. a Cut-in phase; b intermediate phase; c cut-out phase

Fig. 5 Simulation results of milling force

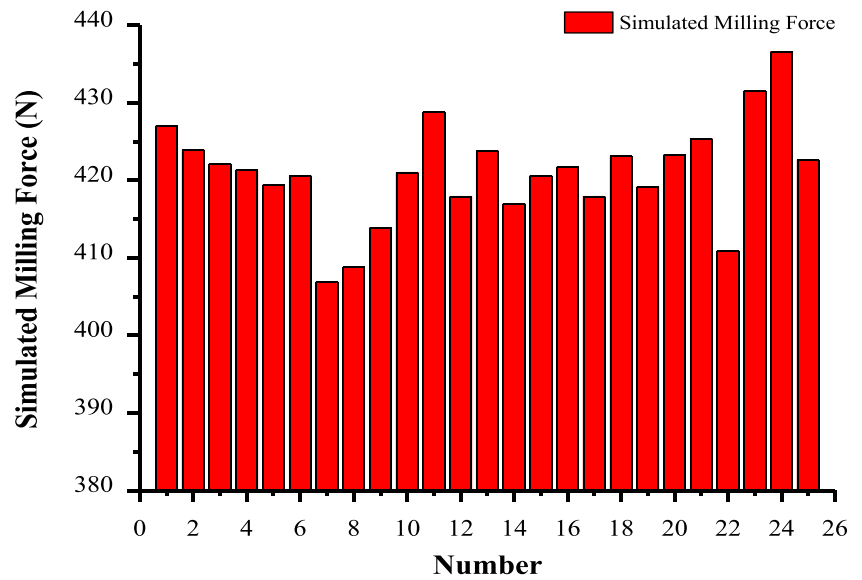
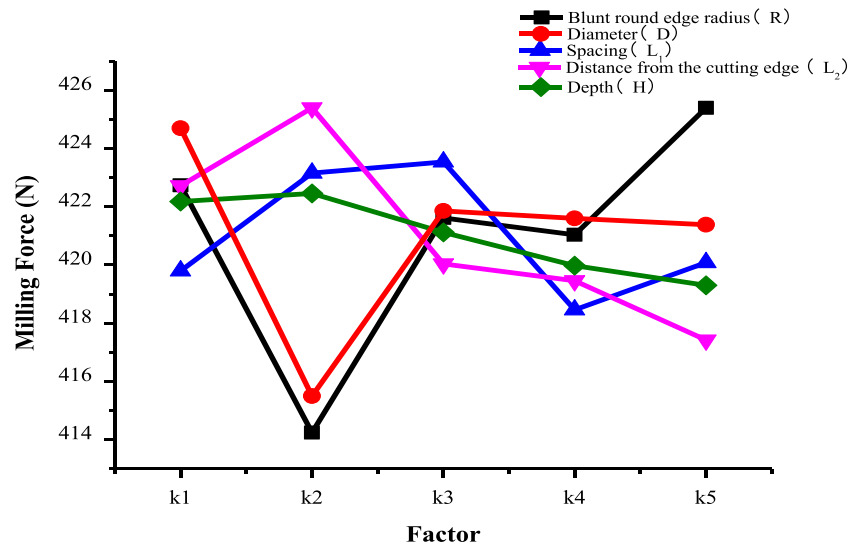


Table 2 Range analysis

Experimental parameters	Blunt round edge radius $R/\mu\text{m}$	Diameter $D/\mu\text{m}$	Spacing $L_1/\mu\text{m}$	Distance from the cutting edge $L_2/\mu\text{m}$	Depth $H/\mu\text{m}$
$K_1$	2113.7	2123.5	2099	2113.6	2110.9
$K_2$	2071.2	2077.5	2115.8	2127	2112.3
$K_3$	2108.1	2109.3	2117.7	2100.2	2105.6
$K_4$	2105.2	2108	2092.3	2097.3	2099.9
$K_5$	2127	2106.9	2100.4	2087.1	2096.5
$k_1$	422.74	424.7	419.8	422.72	422.18
$k_2$	414.24	415.5	423.16	425.4	422.46
$k_3$	421.62	421.86	423.54	420.04	421.12
$k_4$	421.04	421.6	418.46	419.46	419.98
$k_5$	425.4	421.38	420.08	417.42	419.3
$R$	11.24	9.2	5.08	7.98	3.16

**Fig. 6** Influence of those factors on the cutting force



force, followed by the diameter, distance to cutting edge, spacing, and depth. The results are the same with those in simulation.

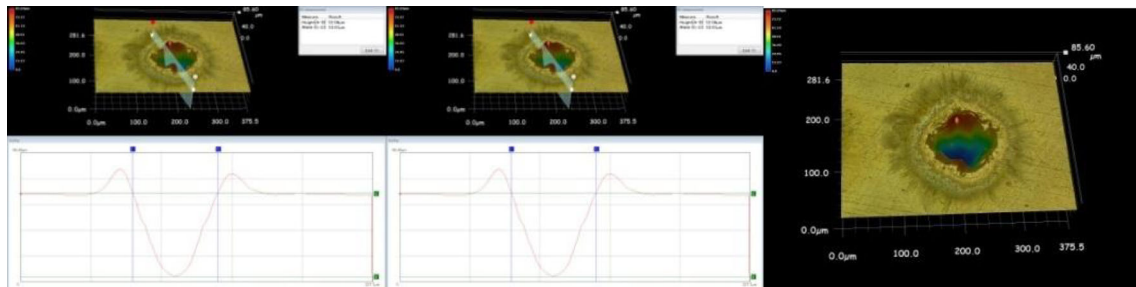
Figure 15 shows the influence of the 5 parameters on the cutting force. Here, the milling force is decreased first and then increased with the increasing radius. When the radius of the blunt round edge is smaller than 40 μm, the cutting edge is too sharp to resist the cutting force, causing the chipping of the cutting edge, resulting in the greater milling force. When the radius is bigger than 40 μm, the

milling force is increased with radius increasing, since the phenomenon of negative rake angle cutting is dominant, resulting in a larger contact area between the cutting edge and chips and larger milling force. Here, the milling force is decreased first and then increased with the increase of micro-texture diameter. When the radius of the diameter is smaller than 40 μm, with the increase of diameter, the chip-holding capacity of micro-texture increases, and the friction between the tool, workpiece, and chip decreases, which leads to the decrease of milling force. When the

**Fig. 7** Micro-textures. **a** Tool of experiment number 1; **b** tool of experiment number 2



a) Tool of experiment number 1 b) Tool of experiment number 2



a) Micro-texture morphology b) Micro-texture front c) Micro-texture side

**Fig. 8** Micro-texture morphology before treatment. **a** Micro-texture morphology; **b** micro-texture front; **c** micro-texture side

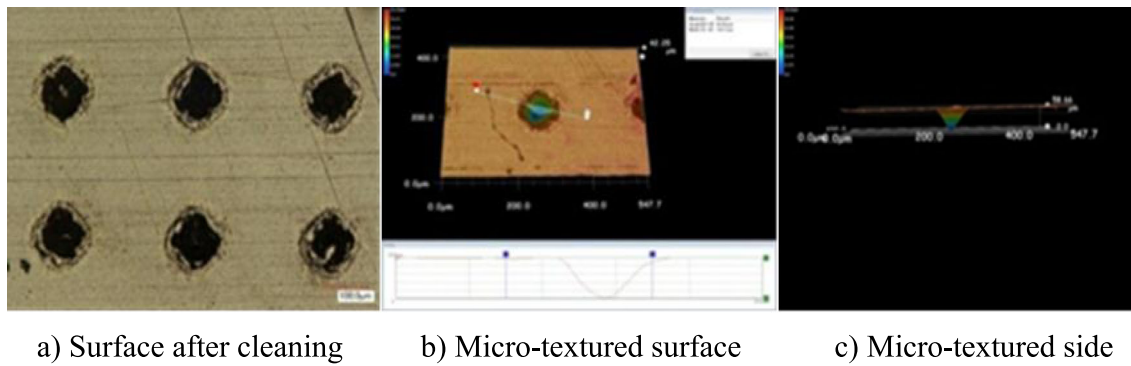


Fig. 9 Morphology observation after treatment. **a** Surface after cleaning; **b** micro-textured surface; **c** micro-textured side

diameter is bigger than 40  $\mu\text{m}$ , the milling force is increased with the increasing diameter, since the contact area between cutter and chip will increase, causing secondary cutting. When the diameter is large enough, the change of milling force is not obvious. Here, the milling force is decreased first and then increased with the increase of micro-texture spacing. When the spacing between micro-textures are too small, the number of micro-textures increases in the unit area, resulting in stress concentration on the surface of micro-textured cutters, which has a certain impact on the structural strength of the cutters and makes the milling force larger. When the spacing is larger than 175  $\mu\text{m}$ , the milling force is increased with spacing increasing slowly, since the contact area between cutter and chip increases slowly. The milling force is decreased first and then increased with the increase of distance from the cutting edge. The minimum milling force occurs when the distance from the cutting edge is equal to 110  $\mu\text{m}$ .

When the distance between micro-texture and cutting edge is too small, the stress concentration will occur near the edge of the micro-texture cutting tool, which will affect the structural strength of the tool. When the distance from the cutting edge is too large, the milling force is increased with distance from the cutting edge, since the effect of friction reduction and friction resistance of micro-texture is not obvious. Here, the milling force is increased first slowly and then decreased with the increase of micro-texture depth. When the depth of micro-texture is small, the ability of micro-texture to collect chips is weak, and the effect of micro-texture is not obvious, resulting in the greater milling force. As the depth of micro-texture continues to increase, the ability of micro-texture to accommodate chips increases, which reduces the friction between chips and tools and workpieces, resulting in the reduction of milling force. When the depth is 80  $\mu\text{m}$ , the minimum milling force appears.

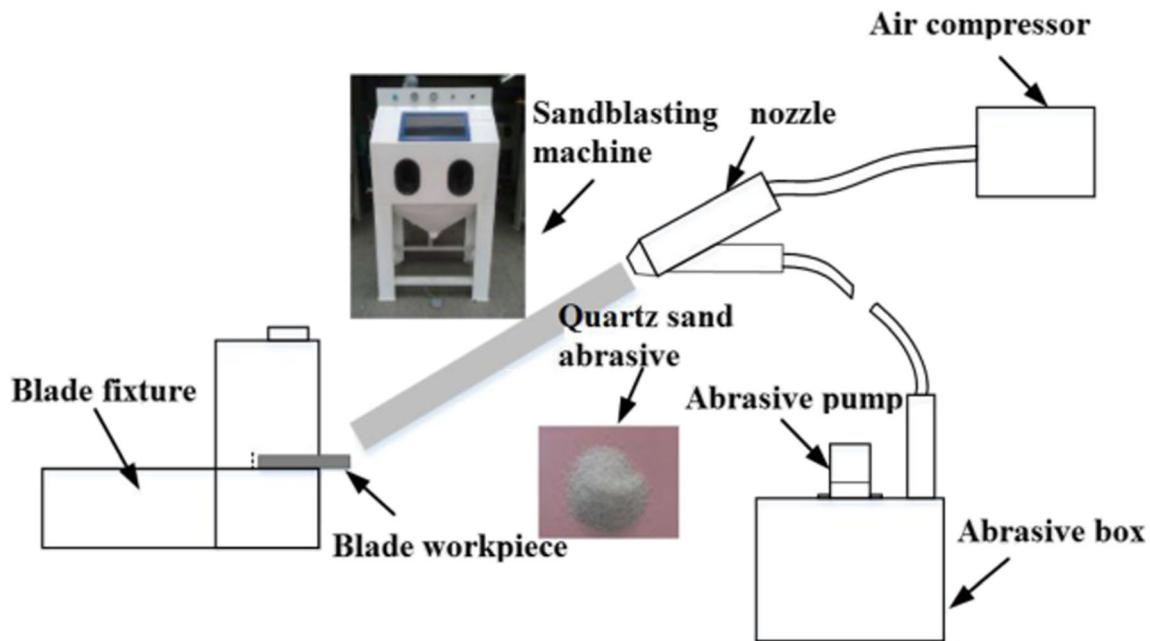
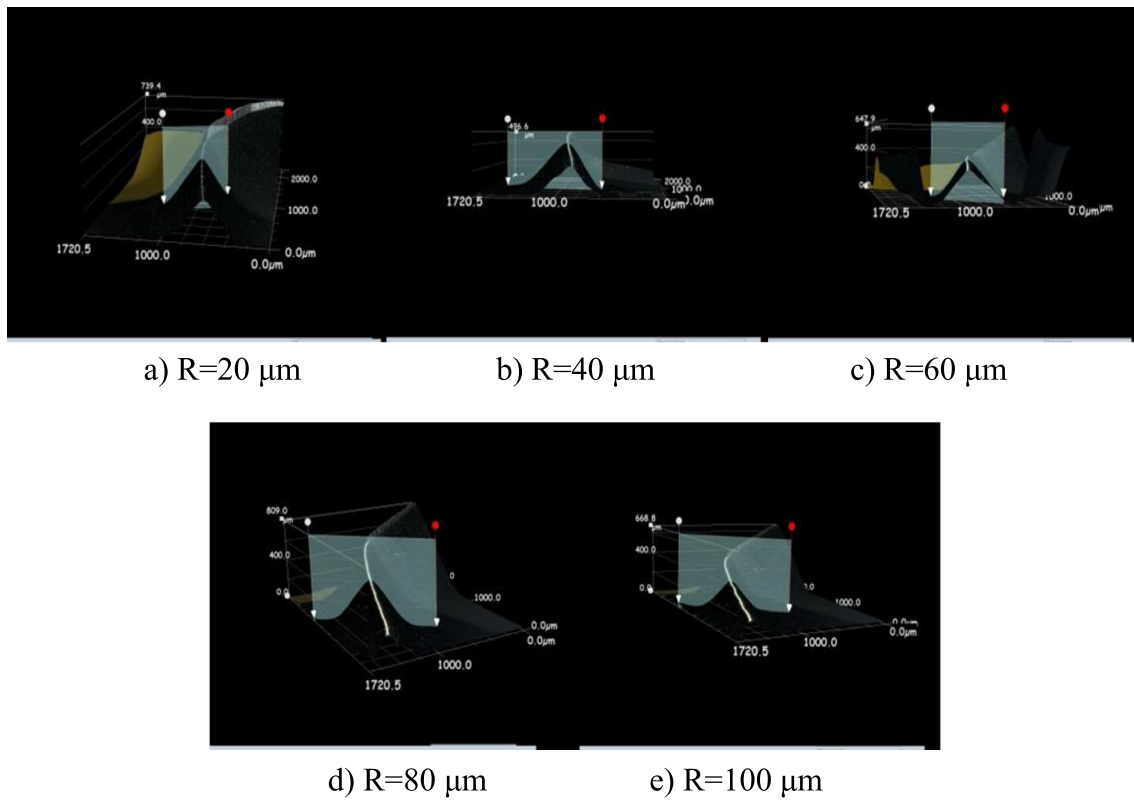
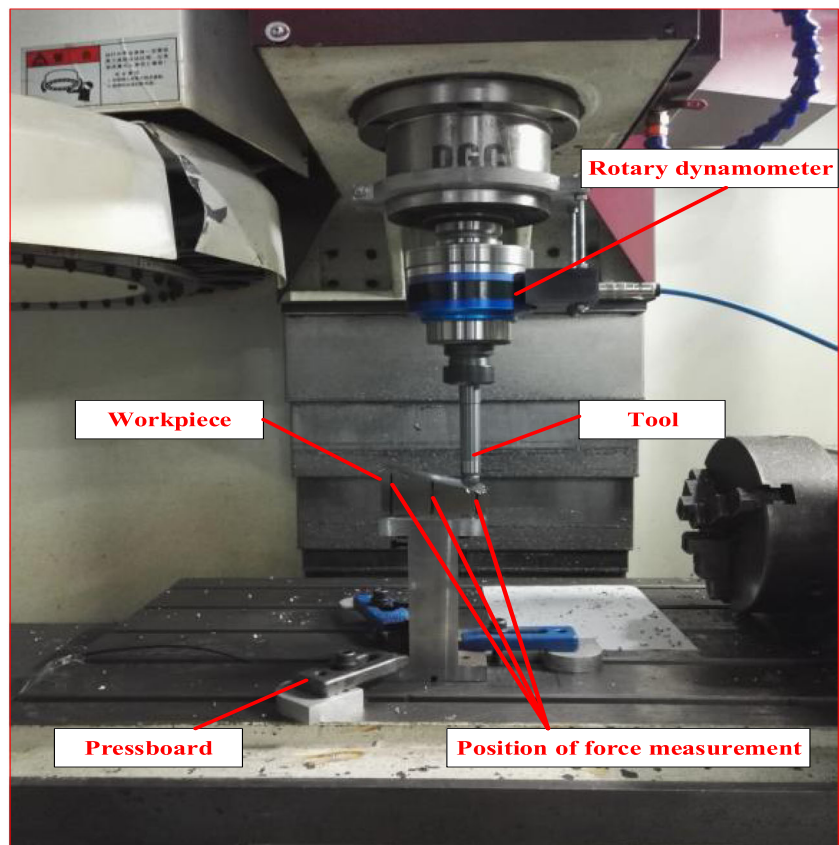


Fig. 10 Machining schematic diagram of the sandblasting machine



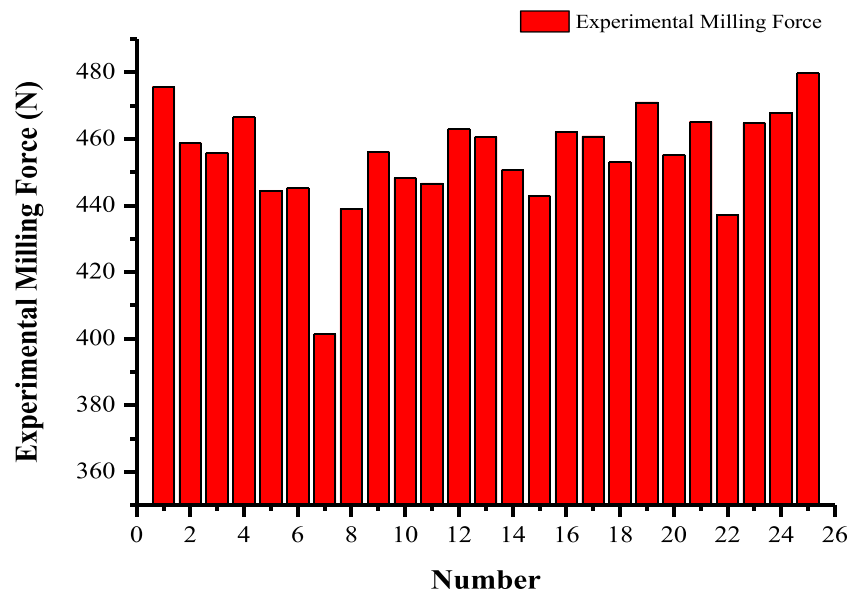
**Fig. 11** 3D measurement of the cutting edge radius. **a**  $R = 20\ \mu\text{m}$ ; **b**  $R = 40\ \mu\text{m}$ ; **c**  $R = 60\ \mu\text{m}$ ; **d**  $R = 80\ \mu\text{m}$ ; **e**  $R = 100\ \mu\text{m}$

**Fig. 12** Tool installation graph





**Fig. 13** Average resultant milling force measured three times



Taking the minimum milling force as a criterion, an optimal combination of parameters can be obtained, i.e.,  $K_2R$ ,  $K_2D$ ,  $K_4L_2$ ,  $K_3L_1$ , and  $K_5H$ , and in details, the optimized parameters refer to a 40- $\mu\text{m}$  radius of the blunt round edge, a 40- $\mu\text{m}$  micro-texture diameter, a 175- $\mu\text{m}$  spacing, a 120- $\mu\text{m}$  distance from the cutting edge, and an 80- $\mu\text{m}$  depth.

#### 4 GA-based parameter optimization

Based on the data obtained in the experiment in Section 3, a multivariate regression is used to establish the model between cutting force and the 5 parameters. Equation (4-1) is used as the base of the model, and MATLAB is used to obtain the coefficients in the equation, of which result is shown in Eq. (4-2).

$$F = cR^{\alpha_1}D^{\alpha_2}L_1^{\alpha_3}L_2^{\alpha_4}H^{\alpha_5}, \tag{4-1}$$

where  $c$ , the coefficient of the cutting environment, depends on the processing material;  $R$  is the radius of the cutting edge;  $D$  is the micro-texture diameter;  $L_1$  is the spacing;  $L_2$  is the distance from the cutting edge;  $H$  is the depth;  $\alpha_1$ ,  $\alpha_2$ ,  $\alpha_3$ ,  $\alpha_4$ , and  $\alpha_5$  are pending coefficients

$$F = 469.766R^{0.0076}D^{-0.136}L_1^{0.318}L_2^{-0.0938}H^{-0.1472}. \tag{4-2}$$

On top of the established regression equation, a GA is used to optimize the parameters by using a MATLAB toolbox.

The parameters of GA are set as follows: (1) population size: 100; (2) crossover probability: 0.7; (3) mutation probability: 0.001; the range of optimized parameters is shown in

**Fig. 14** Comparison of the simulated and experimental milling forces

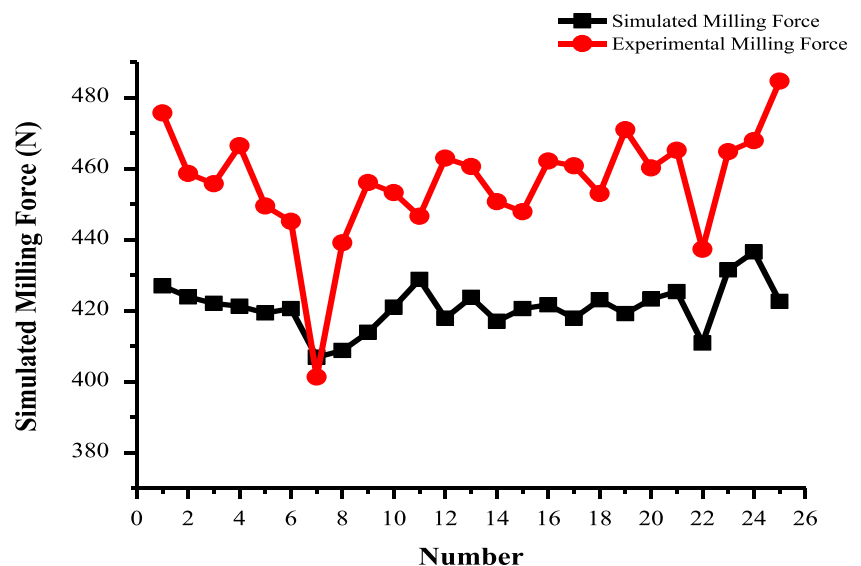


**Table 3** Range analysis

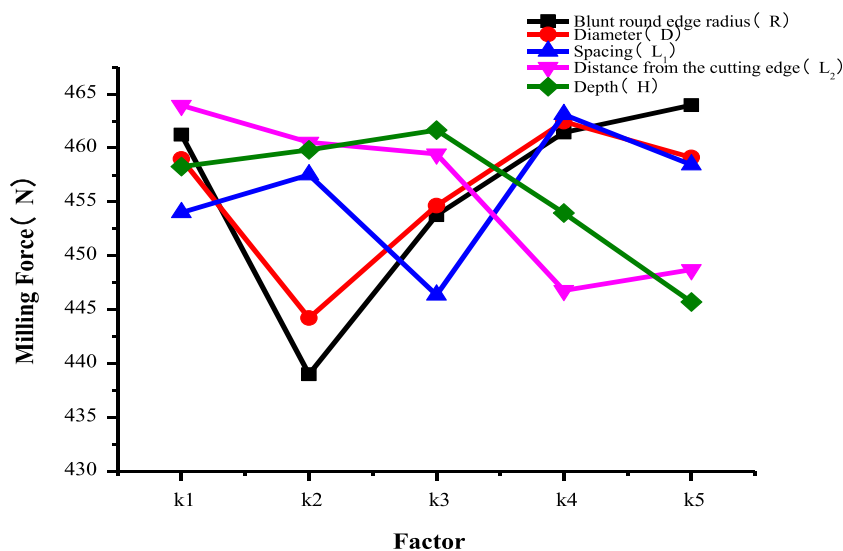
Experimental parameters	Blunt round edge radius $R/mm$	Diameter $D/\mu m$	Spacing $L_1/\mu m$	Distance from the cutting edge $L_2/\mu m$	Depth $H/\mu m$
$K_1$	2306.2	2294.9	2270	2319.8	2291.4
$K_2$	2195	2221.1	2287.6	2302.7	2299.1
$K_3$	2268.8	2273.3	2231.8	2297.2	2308.3
$K_4$	2307.2	2312.2	2315.5	2233.9	2269.8
$K_5$	2319.9	2295.6	2292.2	2243.9	2228.5
$k_1$	461.24	458.98	454	463.96	458.28
$k_2$	439	444.22	457.52	460.54	459.82
$k_3$	453.76	454.66	446.36	459.44	461.66
$k_4$	461.44	462.44	463.1	446.78	453.96
$k_5$	463.98	459.12	458.44	448.7	445.7
$R$	24.98	18.22	16.74	17.18	15.96

Table 4. the fitness of cutting force is stable after 211 generations, as shown in Fig. 16, together with optimized parameter: blunt round edge radius  $40.007 \mu m$ ; micro-texture diameter and spacing  $40 \mu m$  and  $175 \mu m$ , respectively; distance from the cutting edge  $130 \mu m$ ; depth  $80 \mu m$ , i.e., a  $40\text{-}\mu m$  blunt round edge radius, a  $40\text{-}\mu m$  micro-texture diameter, a  $175\text{-}\mu m$  spacing, a  $130\text{-}\mu m$  distance to cutting edge, and a  $80\text{-}\mu m$  depth.

### 5 Comparison of parameters obtained in FEM, experiment, and GA

The optimal parameter combinations obtained from the simulation, experimental results, and GA-based optimization are compared experimentally, by using the same set in Section 3. The related tool parameters are shown in Table 5, in which A, B, and C are the tool obtained in the FEM (Section 2), the experiment

**Fig. 15** Milling factors



**Table 4** Range of parameters

Factor value	Blunt round edge radius $R/mm$	Diameter $D/\mu m$	Spacing $L_1/\mu m$	Distance from the cutting edge $L_1/\mu m$	Depth $H/\mu m$
Upper limitation	100	70	225	130	80
Lower limitation	20	30	125	90	40

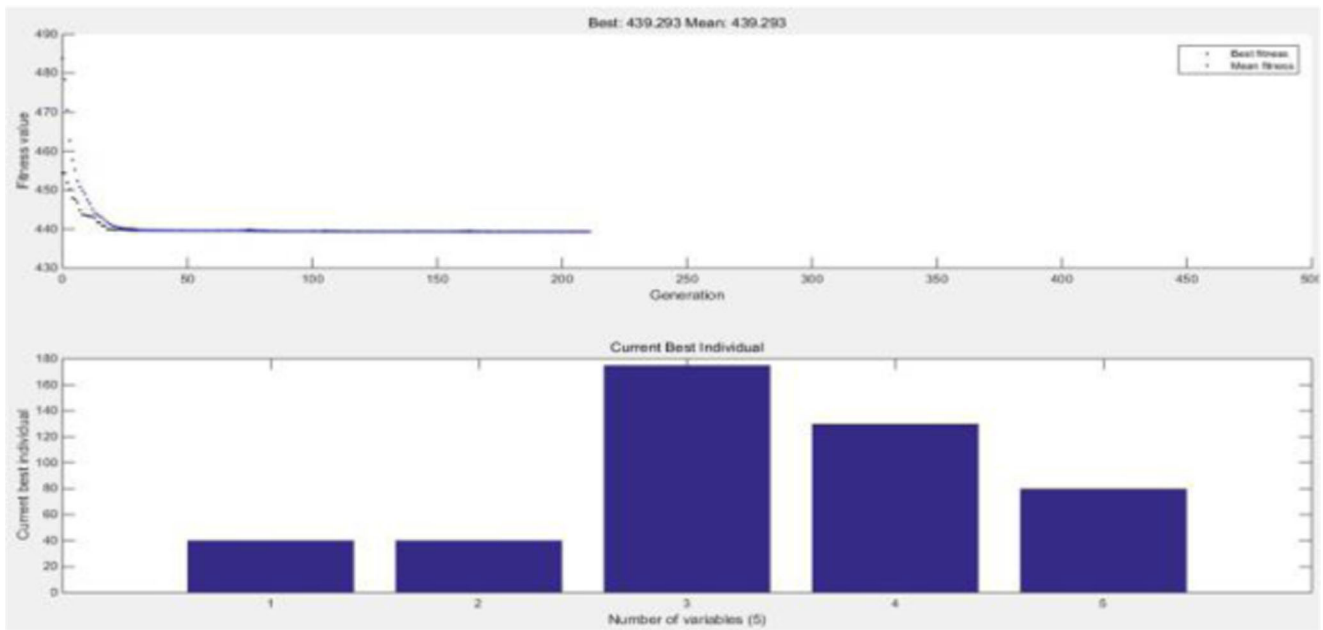


Fig. 16 Genetic algorithm parameter optimization result

(Section 3), and GA-based optimization (Section 4), respectively. The results of the experiment are shown in Table 6, and in general, there are no significant differences between the milling force values, the biggest force is 2.891%  $((418.6 - 406.5) / 418.6)$  larger than the smallest one. The largest force is obtained under tool A, and the smallest force is under tool B. Therefore, the optimized parameters refer to a 40- $\mu\text{m}$  radius of the blunt round edge, a 40- $\mu\text{m}$  micro-texture diameter, a 175- $\mu\text{m}$  spacing, a 120- $\mu\text{m}$  distance from the cutting edge, and an 80- $\mu\text{m}$  depth.

### 6 Conclusion

This paper presents the research on influence of tool radius of a blunt round edge and the micro-texture parameters on

cutting force in a milling operation by using FEM, experiment, and GA-based optimization. The optimized tool parameters obtained in the three methods are compared in a separate experiment. The major contributions of this research are as follows:

1. In terms of the influence on the cutting force, a blunt round edge radius is the biggest one, followed by the diameter, distance to cutting edge, spacing, and depth. Therefore, when designing a ball-end mill with a micro-textured surface and a blunt round edge, the cutting edge radius of the tool has the highest priority, while the depth of the micro-texture is given the lowest priority.
2. In the case of milling titanium alloys, Ti6Al4V, the optimal parameter combination is as follows: a 40- $\mu\text{m}$  blunt

Table 5 Experimental tool parameters

Tool	Blunt round edge radius $R/\mu\text{m}$	Diameter $D/\mu\text{m}$	Spacing $L_1/\mu\text{m}$	Distance from the cutting tool $L_2/\mu\text{m}$	Depth $H/\mu\text{m}$
A	40	40	200	130	80
B	40	40	175	120	80
C	40	40	175	130	80

Table 6 Experimental results

Tool	First measurement $N$	Second measurement $N$	Third measurement $N$	Average value $N$
A	426.2	417.9	411.3	418.6
B	406.3	397.5	415.7	406.5
C	409.7	416.6	405.3	410.9

round edge radius, a 40- $\mu\text{m}$  micro-texture diameter, a 175- $\mu\text{m}$  spacing, a 120- $\mu\text{m}$  distance to cutting edge, and an 80- $\mu\text{m}$  depth.

## References

- Wang HY, Guo ZM, Lu BX, Zhang C (2017) Industrialized production technology of powder metallurgy (PM) titanium and titanium alloy. *Titan Ind Prog* 34(01):1–5
- Fei YJ (2017) Application of titanium and titanium alloy materials. *Adv Mater Ind* 03(05):15–18
- Qi BY (2011) Research on cooling/lubrication technology of green cutting of titanium alloy using surface micro-texture cutting tool. Nanjing University of Aeronautics and Astronautics, The Graduate School, Nanjing, pp 12–14
- Zheng WJ, Huang Q, Zhao XF, Zhou YB (2014) Finite element analysis on influence of rounded cutting edge radius of milling cutter to cutting property. *Coal Mine Mach* 35(10):125–127
- Yang S, Tong X, Liu XL, Ji W, Zhang YH (2018) Investigation on the characteristic of forces of the tool edge in finish machining of titanium alloys. *Int J Adv Manuf Technol* 96:2431–2441
- Obikawa T, Kamio A, Takaoka H, Osada A (2011) Micro-texture at the coated tool face for high performance cutting. *Int J Mach Tools Manuf* 51:966–972
- Wan QF, Lei YY, Yang H, Tao H (2014) Finite element analysis of tool edge roundness based on ABAQUS. *J Xihua Univ Nat Sci* 33(02):63–66
- Cao ZY (2008) Fundamental research on machine tool, cutting tool and cutting mechanism for micro-milling. Nanjing University of Aeronautics and Astronautics, The Graduate School, Nanjing, pp 59–86
- Ezugwu EO, Bonney J, Da Silva RB, Çakir O (2007) Surface integrity of finished turned Ti-6Al-4V alloy with PCD tools using conventional and high pressure coolant supplies. *Int J Mach Tools Manuf* 47:884–891
- Kawasegi N, Sugimori H, Morimoto H, Morita N, Hori M (2009) Development of cutting tools with microscale and nanoscale textures to improve frictional behavior. *Precis Eng* 33:248–254
- Wu YX (1983) The role of the radius of the cutting edge in micro-cutting. *Proc Equip* 01:1–5
- She XR, Su M, LingHu KJ (2015) Influence of cutting parameters and rounded edge radius on milling temperature of 45 steel. *Mod Manuf Proc Equip* 05:22–25
- Wu Z, Deng JX, Lian YS, Cheng HW, Yan GY (2012) Development and perspective of surface textured cutting tool. *Aeronaut Manuf Tech* 10:32–37
- Enomoto T, Sugihara T (2010) Improving anti-adhesive properties of cutting tool surfaces by nano-/micro-textures. *CIRP Ann - Manuf Technol* 59:597–600
- Enomoto T, Sugihara T (2011) Improvement of anti-adhesive properties of cutting tool by nano/micro textures and its mechanism. *Procedia Eng* 19:100–105
- Enomoto T, Sugihara T, Yukinaga S, Yukinaga S, Satak U (2012) Highly wear-resistant cutting tools with textured surfaces in steel cutting. *CIRP Ann - Manuf Technol* 61:571–574
- Sugihara T, Enomoto T (2013) Crater and flank wear resistance of cutting tools having micro surfaces. *Precis Eng* 37:888–896
- Sugihara T, Enomoto T (2012) Improving anti-adhesion in aluminum alloy cutting by micro stripe texture. *Precis Eng* 36:229–237
- Koshy P, Tovey J (2011) Performance of electrical discharge textured cutting tools. *CIRP Ann - Manuf Technol* 60:153–156
- Wu KZ, Chen YJ, Zhu DD, Chen DH, Zhou FQ, Zheng W (2005) Application of friction-reducing groove on insert with 3D chip-breaking groove. *Tool Eng* 39(5):53–55
- Yin SB, Ji W, He GH, Liu XL, Wang LH (2018) Experimental evaluation on texture of flank face on tool wear in chamfer milling of stainless steel. *Int J Adv Manuf Technol* 99:2929–2937
- Yang SC, Liu WW, Zhang YH, Wan Q (2018) Experimental evaluation on micro-texture parameters of carbide ball-nosed end mill in machining of titanium alloy. *Int J Adv Manuf Technol* 96:1579–1589
- Li Q, Yang SC, Zhang YH, Zhou YZ, Cui JT (2018) Evaluation of the machinability of titanium alloy using a micro-textured ball end milling cutter. *Int J Adv Manuf Technol* 98:2083–2092

**Publisher's note** Springer Nature remains neutral with regard to jurisdictional claims in published maps and institutional affiliations.